NANO LETTERS

2006
Vol. 6, No. 9
1880−1886

Transparent, Conductive, and Flexible Carbon Nanotube Films and Their Application in Organic Light-Emitting Diodes

Daihua Zhang,[†,§] Koungmin Ryu,[†,§] Xiaolei Liu,[†] Evgueni Polikarpov,[‡] James Ly,[‡] Mark E. Tompson,[‡] and Chongwu Zhou*[,†]

Department of E.E.-Electrophysics and Department of Chemistry, University of Southern California, Los Angeles, California 90089

Received April 16, 2006; Revised Manuscript Received June 21, 2006

ABSTRACT

We have carried out comparative studies on transparent conductive thin films made with two kinds of commercial carbon nanotubes: HiPCO and arc-discharge nanotubes. These films have been further exploited as hole-injection electrodes for organic light-emitting diodes (OLEDs) on both rigid glass and flexible substrates. Our experiments reveal that films based on arc-discharge nanotubes are overwhelmingly better than HiPCO-nanotube-based films in all of the critical aspects, including surface roughness, sheet resistance, and transparency. Further improvement in arc-discharge nanotube films has been achieved by using PEDOT passivation for better surface smoothness and using $SOCl_2$ doping for lower sheet resistance. The optimized films show a typical sheet resistance of ∼160 Ω/□ at 87% transparency and have been used successfully to make OLEDs with high stabilities and long lifetimes.

Evaluating the potential of carbon nanotubes (CNTs) as the basis of future nanoelectronics technology has been the subject of intense research since their discovery. In contrast, their applications in macroelectronics had received limited attention until three to four years ago when fabrication and purification of macroscopic nanotube products became a relatively mature technique.[1,2] Recently, considerable research on macro-optoelectronics has focused on optimizing the performance of organic light-emitting diodes (OLEDs) by incorporating CNTs into polymer matrixes as a dopant material.[3−9] It is found that the combination of CNTs with polymers offers an attractive route not only for reinforcing polymer films but also for introducing new electronic properties based on morphological modification or electronic interaction between the two components. The effect of CNT doping has been systematically investigated by embedding CNT powders in the emission,[3−6] electron-transport,[7,8] and hole-transport[9] layers of OLEDs (Figure 1a). By introducing additional energy levels or forming carrier traps in the host polymers, the CNT dopant can selectively facilitate or block the transport of charge carriers and effectively improve the OLED performance at optimized dopant concentrations.

In parallel with the research efforts on the CNT−polymer mixtures, continuous CNT films[10,11] could offer a new class of transparent conducting materials that complements indium−tin oxide (ITO) for certain niche applications, including organic light-emitting diodes and organic photovoltaic (OPV) devices. For example, CNT films are superior to ITO in terms of the flexibility because the former can be bent to acute angles without fracture. In addition, although carbon is the most abundant element in nature, the worldwide production of indium is limited, which may soon find difficulty meeting the ever-increasing demand for large-area transparent conductive electrodes. Furthermore, CNT films may offer additional advantages such as tunable electronic properties through chemical treatment and enhanced carrier injection owing to the large surface area and field-enhanced effect at the nanotube tips and surfaces.[12] Although ITO films still lead CNT films in terms of sheet conductance and transparency, the above-mentioned advantages have stimulated significant interest in exploiting carbon nanotube films as transparent conductive electrodes for OLEDs.

Pioneering work has been performed by Zhang et al. using multiwalled nanotube films as electrodes for OLED devices.[13] In addition, high-quality single-walled nanotube (SWNT) films have been produced using nanotubes synthesized via laser ablation.[10,11] In this paper, we report on comparative studies on transparent conductive thin films and also OLED

* Corresponding author. E-mail: chongwuz@usc.edu.
† Department of E. E.-Electrophysics.
‡ Department of Chemistry.
§ These authors contributed equally.

10.1021/nl0608543 CCC: $33.50
Published on Web 08/12/2006

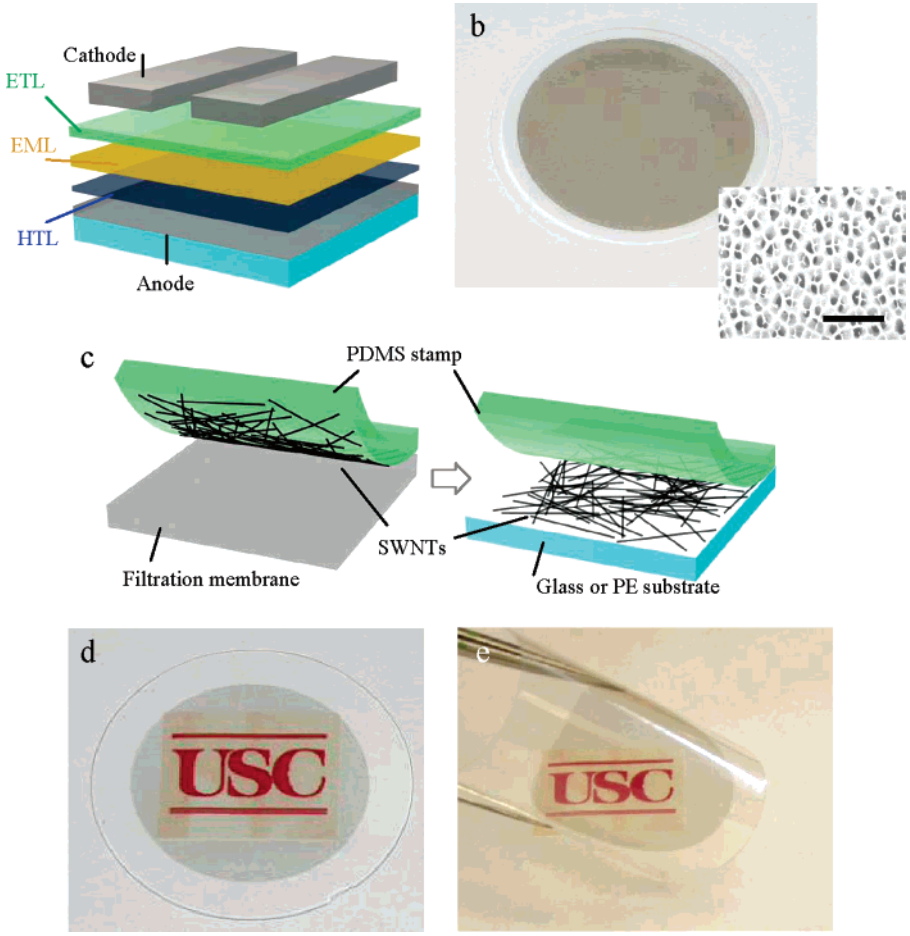

Figure 1. (a) Schematic diagram of a typical multilayer OLED. (b) Photograph of a SWNT film on an alumina filtration membrane. Inset: an SEM image showing the microscopic structure of the porous membrane surface (before SWNT deposition). (c) Illustration of the dry transfer process, in which the SWNT film is peeled off from the filtration membrane using a PDMS stamp and successively printed on a rigid or flexible substrate. (d) A transparent 40-nm-thick SWNT film on a glass substrate 2″ in diameter and (e) a flexed SWNT film on a PE sheet. A sheet of paper with printed "USC" was placed underneath the nanotube films to illustrate the transparency.

devices made with two kinds of commercial SWNTs: HiPCO nanotubes (Carbon Nanotechnology Inc.) and arc-discharge nanotubes (P3 nanotubes from Carbon Solutions Inc.). This choice of materials is based on the fact that HiPCO and arc-discharge nanotubes are currently the only two SWNT products commercially available in bulk quantities. Systematic investigation of their transparent networks can therefore provide practical information to interdisciplinary research on carbon nanotubes and organic displays. Our control experiments demonstrate that arc-discharge nanotubes form far more homogeneous and conductive networks than HiPCO nanotubes and result in OLEDs with longer lifetimes when serving as the hole-injection electrodes. We have also performed polymer passivation and $SOCl_2$ doping to further reduce the surface roughness and sheet conductance of the SWNT films. The optimized films show a typical sheet resistance of ~160 Ω/□, 87% transparency, and a surface roughness comparable to that of ITO substrates.

We adopted a vacuum filtration method to prepare SWNT films. The technique was originally developed by de Heer et al.[14] and has been reexamined recently.[10,11] We started by mixing HiPCO and P3 SWNTs with 1 wt % aqueous sodium dodecyl sulfate (SDS) to make a highly dense SWNT suspension with a typical concentration of 1 mg/mL. HiPCO SWNTs are as-produced nanotubes with a purity of 78.2 wt %, whereas P3 SWNTs are purified arc-discharge nanotubes with a purity of 80 wt %. Both types of tubes were used as received without any further purification or intentional doping. The addition of SDS surfactant further improves the solubility of SWNTs by sidewall functionalization. This highly concentrated SWNT suspension was then ultrasonically agitated using a probe sonicator for ~10 min, followed by centrifugation to separate out undissolved SWNT bundles and impurities. To make a uniform SWNT film, the as-produced suspension was further diluted by a factor of 30 with deionized water and filtered through a porous alumina filtration membrane (Whatman, 200 nm pore size, Figure 1b inset). As the solvent went through the pores, the SWNTs were trapped on the membrane surface, forming a homogeneous gray layer (Figure 1b). This film-forming approach leads to greater production efficiency compared to previous methods because one can produce a large quantity of the highly concentrated SWNT suspension. This simplicity is attributed to the use of a probe sonicator, which significantly facilitated the dispersion of SWNTs in the aqueous SDS solvent.

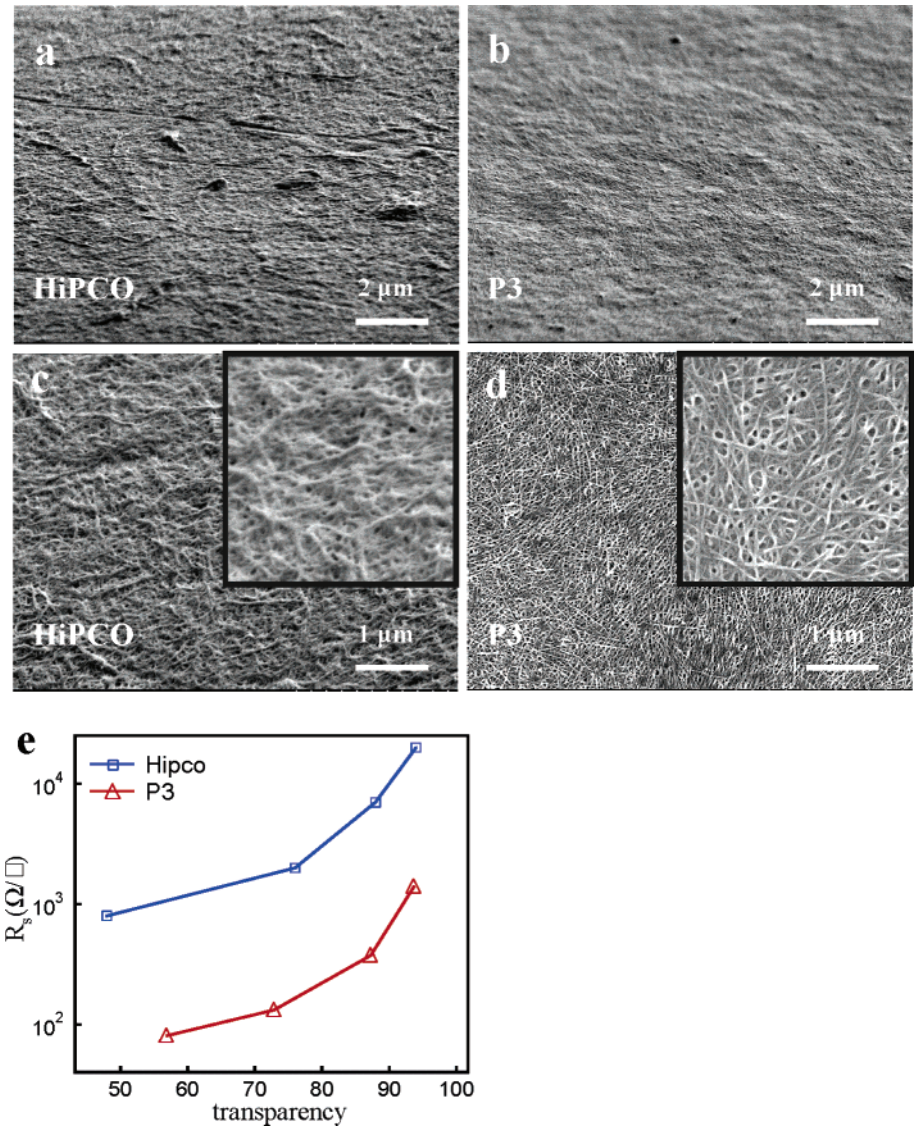

Figure 2. (a and b) SEM images of a HiPCO and a P3 SWNT film taken from a perspective angle (60° from the normal direction), respectively. c and d are top views of the same SWNT films. The inset images (1 μm by 1 μm) are taken at higher magnifications. (e) Sheet resistance vs transparency curves of HiPCO and P3 SWNT films.

Unlike the previous approaches, which require dissolving the filtration membrane in wet chemicals to release the SWNT film,[10] here we use a dry method to transfer the SWNTs from the filtration membrane to target substrates. This dry-transfer approach, initially developed by Zhou et al.,[11] uses an adhesive, soft, and flat poly(dimethysiloxane) (PDMS) stamp to peel the SWNT film off of the filtration membrane and then release it onto a desired substrate, as illustrated in Figure 1c. We note that press printing requires mild heating during contact (100 °C, 1 min) to improve the adhesion of the target substrates. Using this technique, we have demonstrated complete SWNT film transfer to glass (Figure 1d) and flexible polyester (PE) substrates (Figure 1e), which can be subsequently used as transparent conductive electrodes for OLEDs, organic photovoltaic devices, or other optoelectronic devices.

Figure 2 compares the surface morphology and electrical conductance of the as-prepared HiPCO and P3 SWNT films. Figure 2a and b are perspective-view (60° from the normal direction) SEM images of SWNT films made of HiPCO and P3 nanotubes, respectively. Although the P3 SWNTs form a rather dense and homogeneous network, HiPCO nanotube films display a number of "bumps" distributed on the film surface, which presumably result from the impurities or bundled nanotubes in the HiPCO product. The difference in surface quality is also revealed by the top-view SEM images displayed in Figure 2c and d. The HiPCO SWNT film shows a higher roughness level because of the nanotubes and impurities protruding from the surface, whereas P3 nanotubes tend to bind to the supporting substrate conformally, forming a smooth network. Furthermore, we have observed that P3 SWNT films consistently exhibit much higher sheet conductances than HiPCO nanotubes by more than 1 order of magnitude at similar optical transparency, as shown in Figure 2e. The origin of this difference may be related to several factors, including differences in the nanotube dimension, the defect density, the presence of resistive impurities, and the ease of separating bundled nanotubes. A comprehensive

Table 1. Comparison between Pristine Nanotube Films Based on HiPCO and P3 Nanotubes

	roughness (nm)	R_s at 87% transparency (Ω)	lifetime of OLEDs
HiPCO	11	7200	<30 s
P3	7	380	>4−5 hours[a]

[a] This represents a lower limit set by the measurement time we used.

comparison between the two types of commercial SWNTs is shown in Table 1. In the rest of this report, we will focus our discussion on P3 SWNT films, which outperform HiPCO nanotubes in all critical aspects including the surface smoothness, sheet conductance, and the stability of OLED devices, as discussed below.

Further examination of the surface roughness was carried out using atomic force microscopy (AFM). Figure 3a shows a typical AFM image of a P3 SWNT film on glass, confirming the formation of dense and homogeneous network of interconnected SWNTs. The average surface roughness of typical pristine P3 SWNT films is around 7 nm as measured for five different samples with similar thicknesses (~40 nm, determined by AFM at step edges). This degree of roughness compares favorably with that of nanotube films based on HiPCO nanotubes, which have a typical roughness of 11 nm, as listed in Table 1. To further reduce the roughness of the P3 SWNT film and ensure uniform light emission across the OLED surface, we spin-coated a commonly used conductive polymer, poly(3,4-ethylenedioxythiophene) (PEDOT), to smoothen the sample surface. As seen in the AFM image in Figure 3b, the SWNT film shows a pronounced improvement in surface flatness, with a substantially reduced roughness of 3.1 nm after PEDOT spin-coating (100 Å). This degree of surface roughness is comparable to that of standard ITO films, which is 2.4 nm as derived from the AFM image in the Figure 3b inset.

We have performed four-probe dc measurements on four different P3 SWNT films and plotted their sheet resistance (R_s) as a function of film thickness (t) in Figure 3c. To correlate our data with literature results, the sheet resistance was further converted to electrical conductivity, as defined as $\sigma = 1/R_s t$. The σ versus t curve (Figure 3c inset) shows a monotonic increase with a tendency to saturate at greater thicknesses. The highest conductivity is 733 S/cm for the 120 nm film, about two times higher than the saturation conductivity (400 S/cm) of P3 SWNT films prepared by spraying.[15] We note that both values are far below the axial conductivity of 10000−30000 S/cm for SWNT ropes[16] because of the lack of alignment and the presence of highly resistive intertube junctions in the random SWNT networks. In a qualitative sense, the conductivity of the SWNT film is determined by the density of conducting channels in the

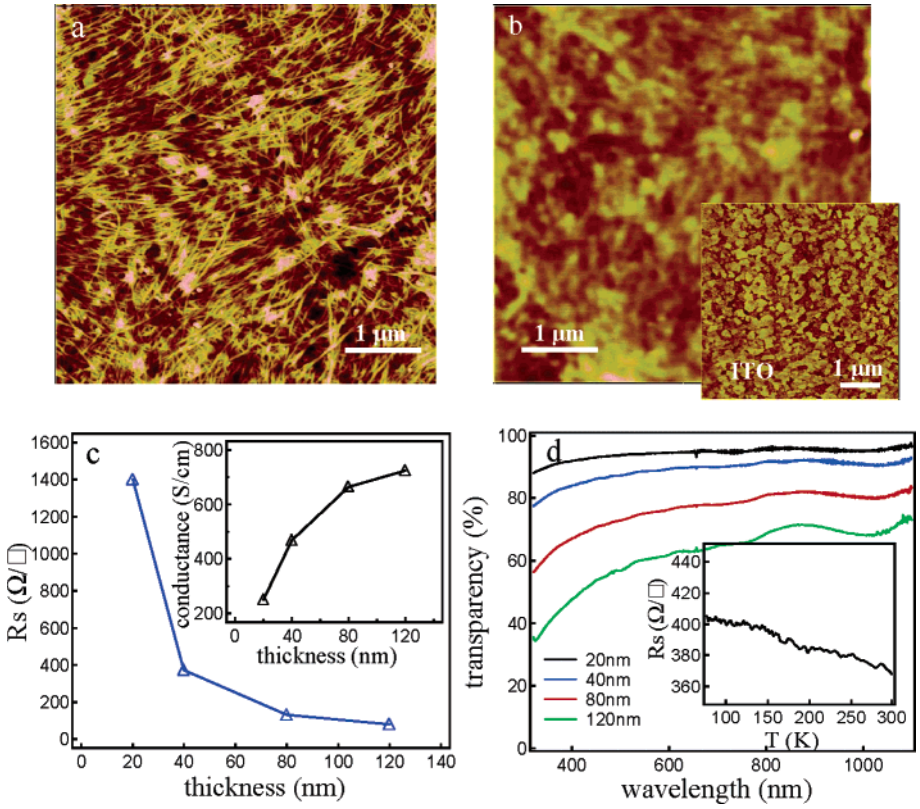

Figure 3. (a) AFM image of a pristine P3 SWNT film. (b) AFM image of a PEDOT-passivated nanotube film showing a surface roughness of 3.1 nm, which is comparable to 2.4 nm roughness of typical ITO substrates (inset). (c) Sheet resistance vs film thickness of P3 SWNT films. Inset: conductivity vs film thickness. (d) Transmittance spectra for SWNT films of thickness 20, 40, 80, and 120 nm. The transmittance of the SWNT films decreases monotonically with the film thickness. The 20 and 40 nm films exhibit sufficiently high transparency (>80%) over a wide spectral range from 300 to 1100 nm. Inset: sheet resistance vs temperature curve taken with a SWNT film of 40 nm in thickness.

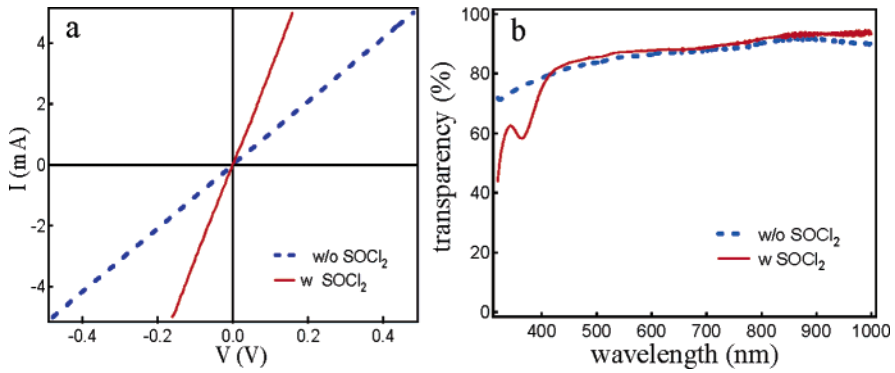

Figure 4. (a) Four-probe $I-V$ curves taken on a 40 nm SWNT film before (dashed) and after (solid line) $SOCl_2$ treatment, indicating a decrease in sheet resistance by a factor of ~2.4. (b) Transmittance spectra of a pristine (dashed) and a $SOCl_2$-treated (solid line) sample.

random network, which is expected to scale as the concentration of low-resistance intertube junctions formed by metallic SWNTs. The semiconductive−semiconductive and metallic−semiconductive intertube junctions, in comparison, make less contribution to the overall conductivity because of the high Schottky barriers formed at the interfaces. Adding SWNTs into an initially sparse network causes significant increase in the concentration of the metallic−metallic junctions, resulting in the sharp increase in conductivity at small thicknesses. As the SWNT network becomes increasingly compact, the concentration of such conductive junctions tends to saturate in thick films, which eventually leads to the saturation in electrical conductivity.

In comparison with the saturation conductivity of sprayed P3 SWNT films (400 S/cm),[15] the higher conductivity (733 S/cm) observed in our measurements is a result of the press-printing method we adopted, which produces more compact SWNT networks compared to the spray approach.[15] The above microscopic view of the SWNT film conductivity is also supported by the temperature dependence measurement shown in the Figure 3d inset, in which the sheet resistance of the 40 nm film shows a very slight increase (10%) as the temperature decreases from 290 to 77 K. Such nonmetallic behavior and the weak temperature dependence are attributed to the series conduction through the metallic SWNTs that are interrupted by small tunnel barriers at the junctions. In Figure 3d, we present the transmittance spectra of the four SWNT films. Within the spectrum range from 300 to 1100 nm, the transmittance shows a monotonic increase in the visible region and becomes relatively flat in the near-infrared region. The 20 and 40 nm films exhibit sufficiently high transmittance to visible light (93% and 87% at 520 nm), which is comparable to that of typical ITO films (~90%).

OLED electrodes require high conductivity to distribute a uniform electrical potential across the polymer surface. To enhance the conductivity of the SWNT films while retaining their high transparency, we have carried out chemical doping using thionyl chloride ($SOCl_2$), a liquid organic solvent with remarkable reactivity toward graphite surface and SWNTs. The $SOCl_2$ treatment involved immersing the P3 SWNT films in $SOCl_2$ (Aldrich) for 12 h followed by drying in N_2 flow. Figure 4a compares the four-probe $I-V$ curves taken before and after the $SOCl_2$ incubation, in which the treated film shows a significant increase in conductance by a factor of 2.4. Such an effect has been attributed to the strongly oxidizing nature of $SOCl_2$, which exhibits remarkable electron-withdrawing ability when adsorbed on the surface of SWNTs.[17] In fact, the conductivity enhancement effect is not limited to p-type semiconductive SWNTs. Theoretical work[17] has suggested that the significant charge transfer induced by $SOCl_2$ (~0.1 electrons per adsorbate) could also enable Fermi-level shifting into the van Hove singularity region of metallic SWNTs, resulting in a substantial increase in the density of states at the Fermi level. Moreover, we find that despite the significant modification in their electrical properties, the treatment with $SOCl_2$ has a negligible effect on the optical adsorption of SWNTs in the visible region. This has been demonstrated in Figure 4b by comparing the transmittance spectrum of the $SOCl_2$-treated sample with that of a pristine P3 SWNT film. With this doping technique, the optimized films show a typical sheet resistance of ~160 Ω/□ at 87% transparency.

Last, we have demonstrated the use of the optimized SWNT films as hole-injection electrodes in OLEDs on both rigid glass and flexible plastic substrates. The device structure is illustrated in Figure 5a. To fabricate multiple pixels on a single device, the continuous SWNT film was first patterned into 1.5-mm-wide stripes by selective O_2 plasma etching. As an optional step, a Ti/Au electrode was deposited at the end of each SWNT stripe to facilitate external connections. PEDOT was then spin-coated on the SWNT film to form a 200-Å-thick hole-injection buffer layer. After annealing in vacuum for 20 min, 500 Å *N*,*N*′-di-[(1-naphthalenyl)-*N*,*N*′-diphenyl]-1, 1′-biphenyl)4,4′-diamine (NPD) and 500 Å tris (8-hydroxyquinolinato) aluminum (Alq_3) were successively deposited via thermal evaporation, forming the hole-transport and emission layers of the OLED. In the final step, the top cathodes were added by consecutive deposition of 10 Å LiF and 1200 Å Al through a shadow mask. A photograph of the completed device (on glass substrate) is shown in the upper-left inset of Figure 5a.

Figure 5b shows the photoluminescence spectrum of Alq_3, with a single peak centered at 520 nm. We recall that the transparency of the SWNT electrode (40 nm thick) at this wavelength is about 87% according to the transmittance spectra in Figure 3d. The current−voltage curve of the OLED was recorded in Figure 5c with a Keithley 2400 source-meter. The current density, derived using a device area of 2 mm^2,

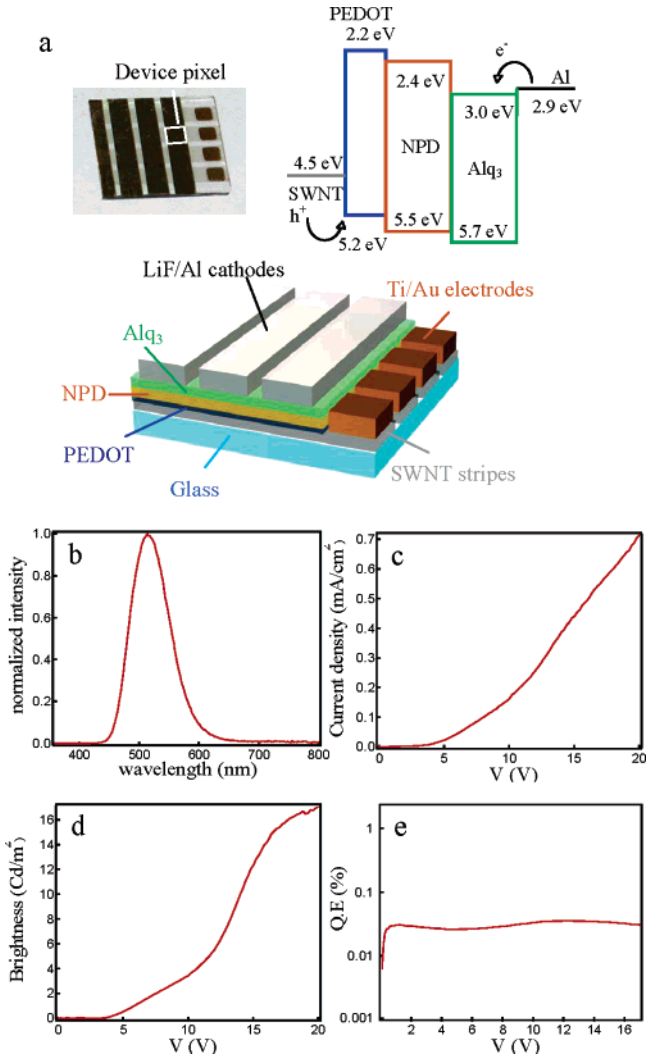

Figure 5. (a) Structure of the OLED device employed for the present study. The device consists of multiple layers of patterned SWNT film (40 nm), PEDOT (10 nm), NPD (50 nm), Alq_3 (50 nm), and LiF(10 Å)/Al (1500 Å). The energy diagram of the device is illustrated in the upper-right inset. The upper-left inset shows a photograph of a completed device fabricated on a glass substrate. (b) Photoluminescence spectrum of the Alq_3 coating. (c) Current density vs voltage bias curve recorded on one device pixel. (d) Brightness vs voltage bias. The device shows a threshold voltage of ~5 V and a maximum brightness of 17 Cd/m^2. (e) Quantum efficiency as a function of current density.

showed a monotonic but nonlinear increase with the voltage bias and reaches 0.7 mA/cm^2 at 20 V. An increase in brightness was accompanied with increasing current density, as measured using a Newport optical meter (Model 1835C). Detailed luminance characterization showed a threshold voltage of 5 V and a brightness of 17 cd/m^2 at 20 V (Figure 5d). Figure 5e plots the quantum efficiency as a function of voltage bias, which varied between 0.21% and 0.34% within a wide bias range from 0.6 to 20 V.

All of the OLED devices based on P3 nanotube films exhibited high stability and long lifetime because no degradation in light emission was observed within four to 5 h. We stress that this represents a lower limit imposed by the measurement time we used, while the device lifetime can be much longer than 4−5 h. In contrast, similar devices have been made with HiPCO nanotube films, and they typically exhibited a lifetime shorter than 30 s before they became either open or short circuits. This remarkable difference is a combined effect of the difference in surface roughness and sheet conductance. As shown in Figure 2, HiPCO films are typically much rougher than P3 films, and the "bumps" in the HiPCO films can easily lead to local heating and filament formation, and eventually result in thermal damage and short/open circuits. The relatively high sheet resistance of the HiPCO films may further hamper the reliability of the OLED devices because higher voltage is needed to operate the HiPCO-based OLED devices than the P3-based counterparts. In addition, we note that even for devices based on P3 nanotube films, the observed current density and brightness are lower than those of typical ITO-based OLEDs by 1−2 orders of magnitude made in our own lab. This may be related to both the higher sheet resistance of the nanotube films and the lower work function of nanotubes (~4.5 eV for nanotubes vs ~4.8 eV for ITO), which leads to a higher hole-injection barrier (as shown in the energy diagram in the Figure 5a inset) and also accounts for the suppressed current density and brightness observed in our studies. Extensive chemical approaches are being investigated in order to further reduce the sheet resistance and effectively modify the electrical properties of the SWNT films. We are also exploring the use of other deposition methods for the molecular organic materials, such as organic vapor phase deposition, which give conformal coatings on highly irregular surfaces, such as the bare SWNT films (i.e., not coated with PEDOT-PSS). Optimization of the device structures should eventually lead to nanotube-film-based OLEDs with performances comparable to those of ITO-based OLEDs.

In summary, we have successfully demonstrated the preparation and optimization of highly transparent SWNT films, which were further exploited as the hole-injection electrodes for OLEDs on both rigid glass and flexible substrates. Our experiments reveal that the choice of material is critical for the success of the application because films based on arc-discharge nanotubes are overwhelmingly better than films based on HiPCO nanotubes in all of the critical aspects, including the surface roughness, sheet resistance, and transparency. Further improvement in arc-discharge nanotube films has been achieved by using PEDOT passivation for better surface smoothness and using $SOCl_2$ doping for lower sheet resistance. The optimized films show a typical sheet resistance of ~160 Ω/□ at 87% transparency and have been used successfully to make OLEDs with high stabilities and long lifetimes. Our work reveals the importance of controlling the surface roughness and conductance of nanotube films and may help to pave the way for systematic studies on using commercial nanotubes as transparent conductive electrodes for applications including organic light-emitting diodes and organic photovoltaic devices.

Acknowledgment. We gratefully acknowledge support from an NSF CAREER Award, an NSF-CENS grant, an NSF-NIRT grant, SRC/MARCO Award, the DARPA

MolApps Program (SPAWAR SysCtr San Diego, no. N66001-04-1-8902) as well as the Universal Display Corporation and the Global Photonic Energy Corporation. We are indebted to Prof. George Gruner, Prof. Robert C. Haddon, Prof. Yang Yang, and Mr. Jinsong Huang for their very valuable discussions.

References

(1) Haddon, R. C.; Sippel, J.; Rinzler, A. G. *MRS Bull.* **2004**, *29*, 252.
(2) Chiang, I. W.; Brinson, B. E.; Huang, A. Y. *J. Phys. Chem. B.* **2001**, *105*, 8297.
(3) Xu, Z.; Wu, Y.; Hu, B.; Ivanov, I. N.; Geohegan, D. B. *Appl. Phys. Lett.* **2005**, *87*, 263118.
(4) Kazaoui, S.; Minami, N.; Nalini, B.; Kim, Y.; Takada, N.; Hara, K. *Appl. Phys. Lett.* **2005**, *87*, 211914.
(5) Kim, J.; Kim, M.; Choi, J. *Synth. Met.* **2003**, *139*, 565.
(6) Ha, Y.; You, E.; Kim, B.; Choi, J. *Synth. Met.* **2005**, *153*, 205.
(7) Fournet, P.; Coleman, J. N.; Lahr, B.; Drury, A.; Blau, W. J.; O'Brien, D. F.; Hörhold, H.-H. *J. Appl. Phys.* **2001**, *90*, 969.
(8) Fournet, P.; O'Brien, D. F.; Coleman, J. N.; Hörhold, H.-H.; Blau, W. J. *Synth. Met.* **2001**, *121*, 1683.
(9) Woo, H. S.; Czerw, R.; Webster, S.; Carroll, D. L.; Ballato, J.; Strevens, A. E.; O'Brien, D.; Blau, W. J. *Appl. Phys. Lett.* **2000**, *77*, 1396.
(10) Wu, Z.; Chen, Z.; Du, X.; Logan, J. M.; Sippel, J.; Nikolou, M.; Kamaras, K.; Reynolds, J. R.; Tanner, D. B.; Hebard, A. F.; Rinzler, A. G. *Science* **2004**, *305*, 1273.
(11) Zhou, Y.; Hu, L.; Gruner, G. *Appl. Phys. Lett.* **2006**, *88*, 123109.
(12) Romero, D. B.; Carrard, M.; De Heer, W.; Zuppiroli, L. *Adv. Mater.* **1996**, *8*, 899.
(13) Zhang, M.; Fang, S.; Zakhidov, A. A.; Lee, S. B.; Aliev, A. E.; Williams, C. D.; Atkinson, K. R.; Baughman, R. H. *Science* **2005**, *309*, 1215.
(14) de Heer, W. A.; Bacsa, W. S.; Châtelain, A.; Gerfin, T.; Humphrey-Baker, R.; Forro, L.; Ugarte, D. *Science* **1995**, *268*, 845.
(15) Bekyarova, E.; Itkis, M. E.; Cabrera, N.; Zhao, B.; Yu, A.; Gao, J.; Haddon, R. C. *J. Am. Chem. Soc.* **2005**, *127*, 5990.
(16) Thess, A.; Lee, R.; Nikolaev, P.; Dai, H.; Petit, P.; Robert, J.; Xu, C.; Lee, Y. H.; Kim, S. G.; Rinzler, A. G.; Colbert, D. T.; Scuseria, G. E.; Tomanek, D.; Fischer, J. E.; Smalley, R. E. *Science* **1996**, *273*, 483.
(17) Dettlaff-Weglikowska, U.; Skákalová, V.; Graupner, R.; Jhang, S. H.; Kim, B. H.; Lee, H. J.; Ley, L.; Park, Y. W.; Berber, S.; Tománek, D.; Roth, S. *J. Am. Chem. Soc.* **2005**, *127*, 5125.

NL0608543